Metabolic Engineering 47 (2018) 190–199

Contents lists available at ScienceDirect

Metabolic Engineering

journal homepage: www.elsevier.com/locate/meteng

Elucidation of photoautotrophic carbon flux topology in *Synechocystis* PCC 6803 using genome-scale carbon mapping models

Saratram Gopalakrishnan[a], Himadri B. Pakrasi[b], Costas D. Maranas[a,*]

[a] Department of Chemical Engineering, Pennsylvania State University, University Park, PA, USA
[b] Department of Biology, Washington University in St. Louis, St. Louis, MO 63130, USA

ARTICLE INFO

Keywords:
Metabolic flux analysis
Carbon mapping model
Genome-scale model
Synechocystis
Photoautotrophic metabolism

ABSTRACT

Completeness and accuracy of metabolic mapping models impacts the reliability of flux estimation in photoautotrophic systems. In this study, metabolic fluxes under photoautotrophic growth conditions in the widely-used cyanobacterium *Synechocystis* PCC 6803 are quantified by re-analyzing an existing dataset using genome-scale isotopic instationary ^{13}C-Metabolic Flux Analysis (INST-MFA). The reconstructed carbon mapping model *i*mSyn617 and implemented algorithmic updates afforded an approximately 48% reduction in computation time. The mapping model encompasses 18 novel carbon paths spanning Calvin-Benson-Bassham cycle, photorespiration, an expanded glyoxylate metabolism, and corrinoid biosynthetic pathways and 190 additional metabolites absent in core models currently used for MFA. Flux elucidation reveals that 98% of the fixed carbons is routed towards biomass production with small amounts diverted towards organic acids and glycogen storage. 12% of the fixed carbons are oxidized to CO2 in the TCA cycle and anabolic reactions in peripheral metabolism. Flux elucidation using instationary MFA reveals that these carbons are not re-fixed by RuBisCO and are instead off-gassed as CO_2. A newly discovered modality is the bifurcated topology of glycine metabolism using parts of photorespiration and the phosphoserine pathways to avoid carbon losses associated with glycine oxidation. The TCA cycle is shown to be incomplete with a bifurcated topology. Inactivity of futile cycles and alternate routes results in pathway usage and (in)dispensability predictions consistent with experimental findings. The resolved flux map is consistent with the maximization of biomass yield from fixed carbons as the cellular objective function. Flux prediction departures from the ones obtained with the core model demonstrate the importance of constructing mapping models with global coverage to reliably glean new biological insights using labeled substrates.

1. Introduction

Metabolic engineering of photosynthetic organisms is aimed at the sustainable bioconversion of abundant and inexpensive substrates such as sunlight and CO_2 into valuable products such as biomass (Maurino and Weber, 2013), biofuels (Atsumi et al., 2009), and secondary metabolites (Giuliano, 2014). The efficacy of metabolic engineering interventions is evaluated by measuring internal fluxes via 13C-Metabolic flux analysis (13C-MFA) methods (Metallo et al., 2009; Sauer, 2006; Tang et al., 2009). These methods determine the intracellular flux distributions consistent with experimentally measured metabolite labeling distributions given a stable-isotope-labeled input carbon substrate (Zomorrodi et al., 2012). Having CO_2 as the only carbon substrate in cyanobacterial photoautotrophic metabolism, implies uniformity of metabolite labeling distributions under isotopic steady-state (Shastri and Morgan, 2007). As a consequence of this, flux elucidation under photoautotrophic conditions requires transient labeling experiments and aims to recapitulate metabolite labeling dynamics in addition to steady-state labeling distributions (Young et al., 2008). While this approach presents the opportunity to address key questions pertinent to cyanobacterial metabolism such as (i) completion of the TCA cycle, (ii) utilization of the photorespiratory pathway, (iii) existence of the glyoxylate shunt, and (iv) carbon fixation efficiency, experimental and computational challenges have so far restricted wide applicability resulting in a limited number of isotopic instationary MFA (INST-MFA) studies. These include a demonstration of sub-optimal carbon incorporation in *Synechocystis* PCC 6803 (hereafter *Synechocystis*) (Young et al., 2011) and assessment of TCA cycle functionality (Xiong et al., 2015) using a simplified central metabolic model. Other studies aimed at capturing the metabolic response to nitrogen depletion (Hasunuma et al., 2013) and essentiality of the photorespiratory pathway (Huege et al., 2011) only obtained split ratios using fractional labeling and

* Corresponding author.
E-mail address: costas@psu.edu (C.D. Maranas).

https://doi.org/10.1016/j.ymben.2018.03.008
Received 2 June 2017; Received in revised form 6 March 2018; Accepted 7 March 2018
Available online 09 March 2018

turnover of metabolites as opposed to network-wide fluxes. Targeted flux ratio elucidation in any labeling experiment is vulnerable to errors arising from distal influences (Gopalakrishnan and Maranas, 2015a; McCloskey et al., 2016; Suthers et al., 2007). Moreover, ignoring pre-existing (unlabeled) carbon pools upon reaction lumping in core metabolic models causes the artificial acceleration of labeling dynamics leading to significant disagreements between model predictions and experimental data (Noh and Wiechert, 2011). Furthermore, pool sizes are often not measured despite being co-estimated with fluxes, resulting in poor resolution of most metabolite pools sizes. These factors are likely to bias the analysis of labeling data using core metabolic models, motivating the re-analysis of metabolite labeling dynamics obtained during transient labeling experiments using a genome-scale metabolic mapping (GSMM) model.

The accuracy of flux estimation using a GSMM model is contingent on the curation of the base genome-scale metabolic (GSM) model. The GSM model for *Synechocystis* *i*Syn731 (Saha et al., 2012) accurately predicts 95% of the available gene (non)essentiality data which is better than the prediction capability of the *i*AF1260 model for *E. coli* (Zomorrodi and Maranas, 2010). This safeguards against incorrect flux inference arising from omission of too permissive inclusion of reactions in the model (Gopalakrishnan and Maranas, 2015a). With the availability of a curated GSM model and transient metabolite labeling distributions (Shastri and Morgan, 2007), (i) the construction of a genome-scale metabolic mapping (GSMM) model and (ii) scalability of existing algorithms become the bottlenecks for successful flux elucidation at the genome-scale (Gopalakrishnan and Maranas, 2015b). In addition to the carbon paths contained within core models (Abernathy et al., 2017; Alagesan et al., 2013; Feng et al., 2010; Yang et al., 2002a, 2002b, 2002c; You et al., 2014; Young et al., 2011; Zhang and Bryant, 2011), the GSMM model affords expanded pathway coverage to include glyoxylate metabolism, completion of the TCA cycle, and recycling of by-products of peripheral metabolism such as CO_2, formate, glycolate and acetate. While the most reliable source of atom mapping data is by directly tracing the reaction mechanism, it is not available for most reactions, thus requiring the use of computational procedures such as MCS (Chen et al., 2013), PMCD (Jochum et al., 1980), EC (Morgan, 1965), MWED (Latendresse et al., 2012), and CLCA (Kumar and Maranas, 2014) to infer plausible mappings. Simulation of labeling distributions for a given flux distribution is performed via integration of a system of ordinary differential equations (ODEs) (Noh et al., 2006; Young et al., 2008) upon decomposition of the mapping model using frameworks such as cumomers (Wiechert et al., 1999) or Elementary Metabolite Units (EMUs) (Antoniewicz et al., 2007). Fluxes are estimated as the solution of a non-linear least-squares fitting problem that minimizes the deviation of predicted intracellular metabolite labeling distributions and dynamics from experimental data. Since the analytical solution for the system of ODEs describing labeling dynamics is not tractable, the ODEs must be integrated numerically. Memory requirements limits the use of available integration packages, thus requiring the development of customized integrators. The state-of-the art algorithm (Young et al., 2008) utilizes an exponential integrator in conjunction with a first-order hold equivalent. When expressed in state-space form, the solution to these equations involves the computation of the exponential of a matrix, which scales poorly with network size requiring the development of more efficient algorithms undertaken in this study.

In this paper, genome-scale INST-MFA is performed to glean insights into the metabolic map of photoautotrophically grown *Synechocystis*. A GSMM model *i*mSyn617 for *Synechocystis* is constructed based on the corresponding GSM model *i*Syn731 (Saha et al., 2012) to enable flux elucidation using previously measured metabolite labeling dynamics (Young et al., 2011). The set of active reactions under photoautotrophic growth conditions is identified by performing Flux Variability Analysis (Mahadevan and Schilling, 2003) upon constraining the model with experimentally measured growth and product yields (Young et al., 2011) for growth with bicarbonate as the sole carbon source. The GSMM *i*mSyn617 is constructed to encompass all active reactions involved in carbon balances. Reaction mapping information is assembled from *i*mEco726 (Gopalakrishnan and Maranas, 2015a), reaction mechanisms and the CLCA algorithm (Kumar and Maranas, 2014). *i*mSyn617 is deployed for genome-scale INST-MFA to uncover novel insights into the biology of photoautotrophic growth of *Synechocystis* using the published labeling data for 15 metabolites form central metabolism (Young et al., 2011). We infer that only 88% of the assimilated bicarbonate is fixed via the Calvin-Benson-Bassham (CBB) cycle while the rest is fixed by phosphoenol pyruvate carboxylase (PPC) but eventually off-gassed as CO_2 through malic enzyme, the TCA cycle, and peripheral metabolic pathways. We confirmed that there is no flux through the oxidative pentose phosphate (PP) pathway and that regeneration of pentose phosphates occurs through the transaldolase reaction. With no flux through pyruvate kinase, pyruvate is synthesized indirectly from phosphoenol pyruvate (PEP) via PPC and malic enzyme. Trace flux is observed from α-ketoglutarate (AKG) to succinate indicating dispensability of the lower TCA cycle during photoautotrophic growth. Moreover, the oxygenase reaction of RuBisCO is found to be the primary source of glycine with serine being synthesized directly from 3-phosphoglycerate (3PG). These modalities result in a bifurcated topology of the TCA cycle reactions and serine metabolism enabling maximal conversion of RuBisCO fixed CO_2 to biomass. This analysis confirmed that maximization of biomass yield from fixed carbons explains the allocation of fluxes in the metabolic network in *Synechocystis* as supported by experimental findings.

2. Methods

2.1. Construction of mapping models

The GSM model for *Synechocystis* (*i*Syn731) (Saha et al., 2012) was simplified using Flux Variability Analysis (FVA) (Mahadevan and Schilling, 2003) under photoautotrophic conditions using bicarbonate as the sole carbon source to eliminate all reactions incapable of carrying flux. The feasible solution space was constrained using growth rate and organic acids yield (Young et al., 2011). Photon fluxes are calculated based on experimental lighting conditions described earlier (Nogales et al., 2012). Thermodynamic infeasible cycles (Schellenberger et al., 2011) in the form of isles (Wiechert and Wurzel, 2001) were manually eliminated to further reduce the size of the metabolic model. The phosphoserine pathway was included in accordance with recent genome annotation updates (Klemke et al., 2015). The recently proposed Entner-Doudoroff pathway was excluded from the metabolic model based on its dispensability under photoautotrophic growth conditions and a lack of pathway characterization using tracer experiments (Chen et al., 2016). The phototrophic growth model for *Synechocystis* contains 729 reactions and 679 metabolites. The GSMM model *i*mSyn617 was constructed for *Synechocystis* starting from the existing GSMM for *E. coli*, *i*mEco726 (Gopalakrishnan and Maranas, 2015a). Carbon mapping for 498 reactions were obtained directly from *i*mEco726, spanning glycolysis, pentose phosphate pathway, TCA cycle, biosynthesis of all amino acids except glycine and serine, synthesis of palmitate and stearate, nucleotide biosynthesis, and the synthesis of cofactors: NAD, tetrahydrofolate, and riboflavin. Of the originally 109 unmapped reactions, 96 reactions spanning carbon fixation, photorespiration, glyoxylate metabolism, glycolipid and polyunsaturated fatty acid synthesis, and porphyrin biosynthetic pathways generated metabolites recycled in central metabolism. Atom mapping for 68 unmapped reactions was constructed from the reaction mechanism of each reaction (Supplementary File 1). Mapping for the remaining 41 reactions including spontaneous reactions and those without available mechanisms was obtained using the CLCA algorithm (Kumar and Maranas, 2014; Kumar et al., 2012). Alternate mappings were generated for 49 reactions based on the presence of nine symmetric

metabolites in the cyanobacterial models. Carbon rearrangements within the triose phosphates were identified by carbon path tracing using an EMU-based depth-first search algorithm. All carbon atoms (single and bonded) are represented using their corresponding EMU following a carbon numbering scheme consistent with the IUPAC convention. The metabolic model and the corresponding atom mapping model are made available in Supplementary File 1.

2.2. Algorithmic procedure for flux estimation based on least-squares minimization

Flux and range estimation following EMU decomposition (Antoniewicz et al., 2007) of the mapping model was performed as described earlier (Gopalakrishnan and Maranas, 2015a). The labeling dynamics of 15 central metabolites, spanning sugar phosphates, glycolytic intermediates, and organic acids, utilized for flux estimation was obtained from a previous study (Young et al., 2011) with *Synechocystis* grown under photoautotrophic growth conditions and 50% ^{13}C-bicarbonate tracer. Model decomposition resulted in the identification of 851 EMUs, 156 free fluxes (Wiechert et al., 1999), and 204 pool sizes. Metabolite labeling dynamics was modeled using a system of 8.4×10^5 simultaneous ODEs relating metabolite labeling distributions $\mathbf{X}(t)$ to the initial labeling state, $\mathbf{X}(0)$, the carbon tracer, and the system state transition matrix, **F**, containing fluxes, **v**, and pool sizes, **c**. This system of ODEs simulates 2311 EMU mass fractions and their sensitivity to 367 fitted parameters. The system of equations in continuous time domain was converted to discrete time domain using the procedure described in the Supplementary Methods. The mathematical expressions for the transition matrices, $\mathbf{\Phi}$, $\mathbf{\Gamma}$, and $\mathbf{\Omega}$, in terms of the **F** were obtained by solving the system of ODEs after applying a non-causal first-order hold equivalent (Franklin et al., 1997) as opposed to the previously described state-space form method (Young et al., 2008) so as to improve the scalability of the flux estimation procedure. This resulted in a 7% and 48% reduction in computation time for the core model and the GSM model, respectively. This significance of this improvement is anticipated to increase with model size. The NLP was solved using a modified Levenberg-Marquardt algorithm (Madsen et al., 2004) equipped to handle linear inequality constraints (Gill et al., 1984). The NLP was solved with 100 randomized initial feasible flux distributions and the best solution was chosen for confidence interval calculations owing to the non-convex nature of the objective function. The quality of the obtained flux distribution was evaluated using a $\chi 2$ goodness of fit test to ensure statistical significance of the obtained results. 95% confidence intervals were determined as described earlier (Antoniewicz et al., 2006; Gopalakrishnan and Maranas, 2015a). All fluxes, expressed in mmol/dmol bicarbonate uptake (BCU), are normalized to 100 mmol/gdw-hr HCO_3^- uptake and are reported in Supplementary File 1.

3. Results

This section highlights the novel carbon paths included upon scale-up to a GSMM model and their role in facilitating prediction departures from flux distributions obtained using core models. In addition, flux topologies of pathways absent in the core model are elucidated and their biological implications are discussed.

3.1. New carbon paths covered by mapping model imSyn617

Expansion of pathway coverage in the GSMM model of *Synechocystis* to include glyoxylate, amino acid, lipid, and peripheral metabolism contributes to 18 novel carbon paths not captured by the core model (Fig. 1). These novel paths arise from new carbon skeleton rearrangements, conserved group recycling, and new mechanisms for CO_2 incorporation in *Synechocystis*. Three alternate routes to lower glycolysis are traced through methylglyoxal synthesis, photorespiration, and serine metabolism with identical atom mapping. Two paths via arginine degradation and the GABA shunt are present with atom transitions identical to the lower TCA cycle, indicating the presence of a TCA-like carbon skeleton rearrangement despite the unresolved completion of the TCA cycle (Steinhauser et al., 2012; Yu et al., 2013; Zhang and Bryant, 2011). Carbon recycling from peripheral metabolism occurs via acetate, formate and CO_2. The condensation of the methyl group from S-adenosyl methionine and the δ-carbon of glutamate (GLU-5) in the adenosylcobalamine pathway produces acetate, which is either metabolized via the TCA cycle or channeled into lipid production. Formate is produced during the biosynthesis of tetrahydrofolate (THF), riboflavin, and thiamin pyrophosphate, whereas CO_2 is generated as a byproduct of porphyrin, terpenoid, and pyridoxal phosphate biosynthetic pathways. Formate and CO_2 are also produced as the end products of glyoxylate oxidation via oxalate. Formate is oxidized to CO_2 via formate dehydrogenase, which is eventually reincorporated via RuBisCO and the anaplerotic PPC reaction. The tetrahydrofolate pathway also generates glycolate, which feeds into the photorespiratory pathway. Since *Synechocystis* lacks PEP carboxykinase (PPCK) activity to drive carbon flow from the TCA cycle to lower glycolysis, CO_2 incorporated via PPC is routed to TCA cycle-derived metabolites only. CO_2 is also incorporated via glycine dehydrogenase (GLYDH) in glyoxylate and glycine metabolism in which glycine is synthesized by condensation of one CO_2 and a methenyl group donated by methenyl-THF. This reaction, in conjunction with flux through the photorespiratory pathway contributes to three novel carbon backbone arrangements possibly unique to cyanobacteria (Fig. 2a). It is important to note that these mechanisms both incorporate and off-gas CO_2 atoms of different origin resulting in alteration of labeling distributions of various intracellular metabolites similar to ^{13}C labeling dilution effects seen during aeration of cell cultures (Leighty and Antoniewicz, 2012). However, it appears that net carbon fixation is performed by RuBisCO alone. In addition to carbon skeleton rearrangements, the mapping model reveals the existence of pathways facilitating conserved moiety cycling (E4P and G3P), which are capable of delaying ^{13}C incorporation (Fig. 2b). The comprehensive inventory of carbon paths contained within the GSMM model provides the means for better recapitulation of experimental data and accurate flux elucidation with a high level of detail.

3.2. Comparison of elucidated fluxes between using imSyn617 and core mapping models

The simulated labeling distributions are in much better agreement with experimental data when fitted using *i*mSyn617 (Sum of Squares of Residuals, SSRES = 511.4; Degrees of freedom, DOF = 556) compared to the core model (Young et al., 2011) (SSRES = 684, DOF = 697). The statistical significance of the reduction in SSRES using *i*mSyn617 was assessed using an *F*-test. The F-test provides a way of testing whether the improvement in fit upon model expansion is not due an increased number of parameters but rather due to better capturing of labeled carbon routes through metabolism. The F-statistic is calculated to be 1.335 ($p = 0.012$). This value confirms the statistical significance of the additional parameters introduced in *i*mSyn617 with a confidence level of 95%. Furthermore, the substantially different flux distribution elucidated using *i*mSyn617 associated with the reduced SSRES captures a statistically significant new optimum in the least squares objective function. The improved fit is attributed to the better recapitulation of the labeling dynamics of PEP-167, 3PG-185, and RuBP-309 fragments indicated by a reduction in SSRES (Fig. 3). Because the experimentally measured metabolite labeling distribution and dynamics are inconsistent with the sole action of the CBB cycle (Supplementary Figs. S1 and S2), flux datasets inferred by both models employ compensatory mechanisms to delay the mass shift associated with ^{13}C incorporation. Simplification of reactions in the core model via lumping of linear pathways may accelerate metabolite labeling dynamics (Noh and Wiechert, 2011). As a result, the core model derives unlabeled carbons from glycogen degradation in conjunction with flux through the

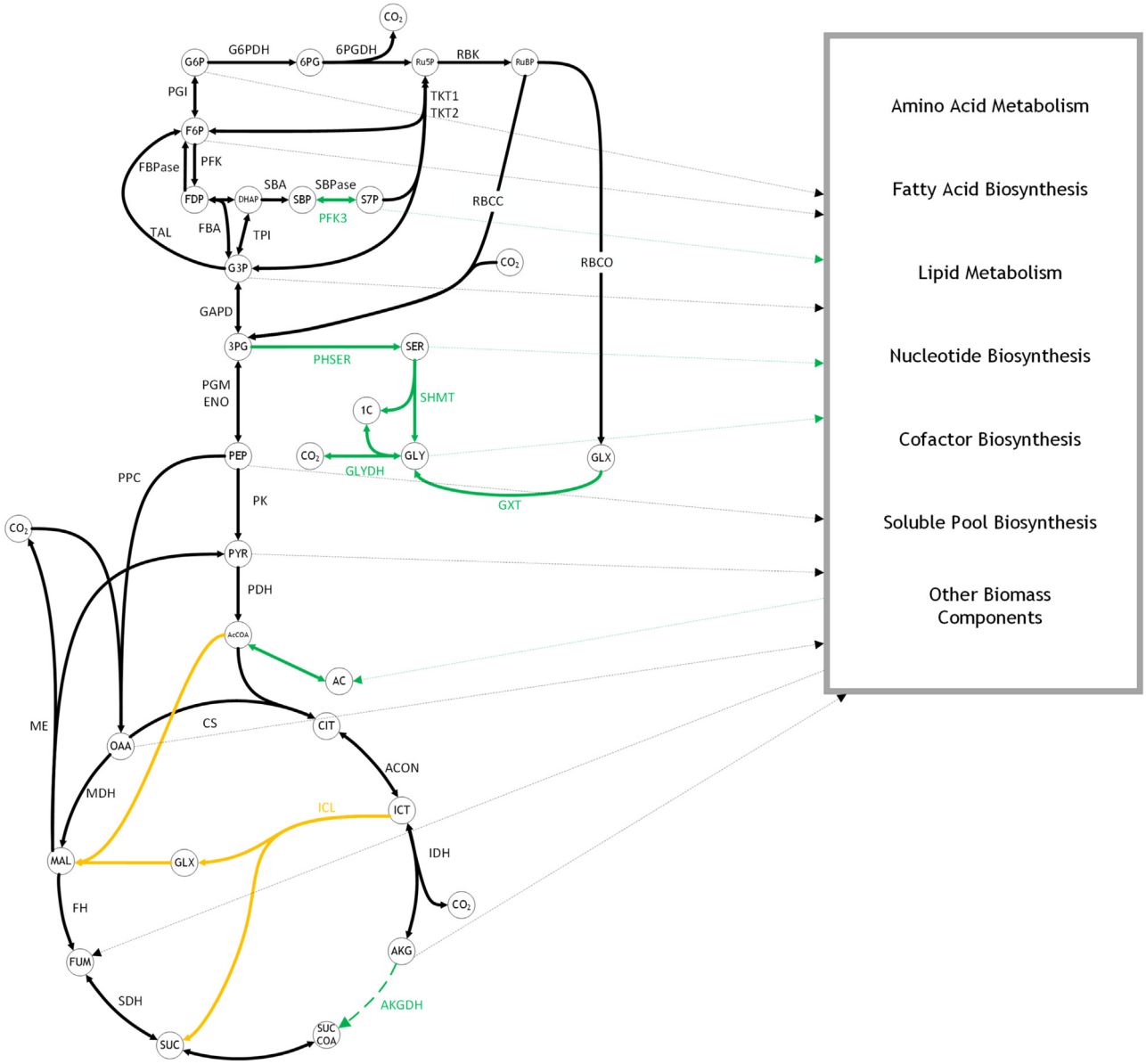

Fig. 1. Representation of central metabolism in *Synechocystis*. The reactions exclusive to the core model and the GSM model are indicated in orange and green, respectively. Metabolite drains for biomass formation and peripheral metabolism are indicated in dashed arrows with GSM-specific interactions indicated in green. Completion of the TCA cycle (AKGDH) is indicated using a dashed green arrow to represent the existence of alternate routes between this pair of metabolites. (For interpretation of the references to color in this figure legend, the reader is referred to the web version of this article).

oxidative pentose phosphate pathway to delay turnover of metabolite pools (Supplementary Fig. S3). In contrast, *i*mSyn617 does not lump reactions and further delays metabolite pool turnover by favoring carbon paths involving conserved moieties (Figs. 2 and 4), thereby affording a reduction in deviation from experimental data using *i*msyn617 (Supplementary Fig. S1). An immediate consequence of this flux redistribution is the dispensability of flux through the oxidative PP pathway (Fig. 4) according to *i*mSyn617. The biomass formation reaction in the core model is approximated using precursors from central metabolism (Shastri and Morgan, 2007) whereas *i*mSyn617 mirrors completely the biomass equation of *i*Syn731 parameterized using experimental measurements (Nogales et al., 2012; Saha et al., 2012). This results in significant differences in metabolite drains between the two models. Overall, differences in labeling dynamics and stoichiometry associated with biomass metabolite drains contribute to stark shifts in estimated central metabolic flux ranges upon scale-up from a core to a genome-scale mapping model (Fig. 4).

Flux elucidation using a GSMM model reveals that only 88% of the assimilated bicarbonate is fixed by RuBisCO (Fig. 4) compared to 120% in the core model. The increased flux through RuBisCO predicted by the core model is attributed to a 16 mmol/dmol bicarbonate uptake (BCU) flux through G6PDH, resulting in a futile cycle between the CBB cycle and the PP pathway, which is shown to be inactive when using *i*mSyn617. This is consistent with experimentally verified dispensability of this pathway inferred from unimpaired growth of the *Synechocystis zwf* mutant under photoautotrophic growth conditions (Scanlan et al., 1995). As a consequence of this, an 83% reduction in the flux through PGI is seen using *i*mSyn617 compared to the core model with the only purpose of generating G6P for glycogen and glycolipid synthesis. *i*mSyn617 leverages the E4P recycling mechanism (Fig. 2b) to delay metabolite labeling dynamics leading to a two-fold increase in flux through SBA and SBP reactions and a flux of 37 mmol/dmol BCU through TAL in *i*mSyn617 compared to the core model. The use of this pathway for regeneration of pentose sugar phosphates results in no flux

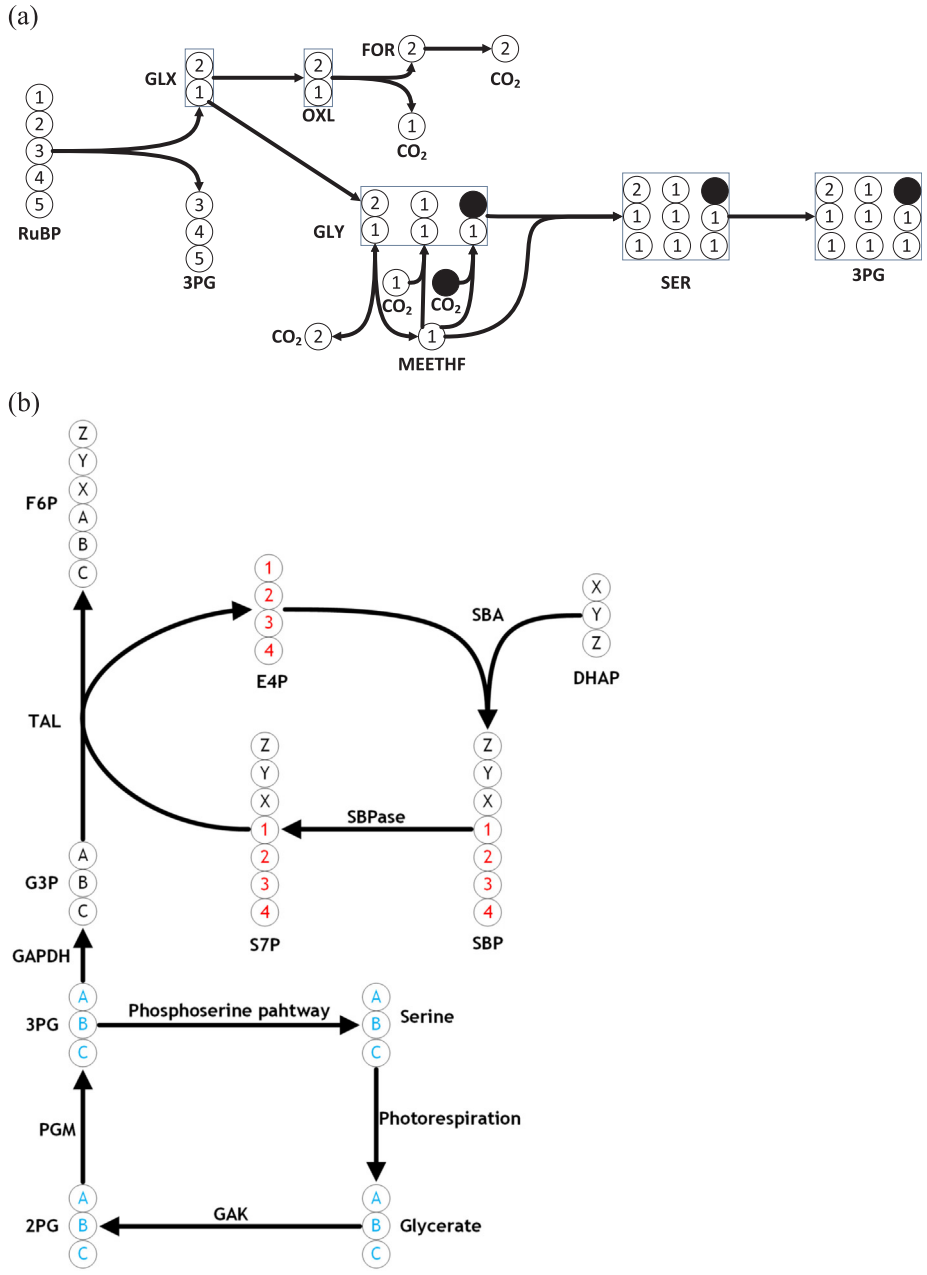

Fig. 2. Carbon incorporation paths and conserved moiety cycling in *i*mSyn617. (a) CO_2 reincorporation via photorespiration. Solid black circles represent reincorporated CO_2 atoms. Reversible glycine degradation is the primary carbon scrambling reaction in this pathway allowing the incorporation of degraded glyoxylate carbons as well as substrate bicarbonate to generate three unique carbon arrangement patterns of 3PG. (b) Recycling of conserved moieties within central metabolism. The conserved E4P moiety (carbon atoms 1,2,3,4) generated due to the interaction between TAL from the non-oxidative PP pathway and SBA and SBPase from the regeneration phase of the CBB cycle is indicated in red whereas the conserved triose phosphate moiety (carbons atoms A, B,C) recycled between the serine biosynthetic pathway, photorespiration, and lower glycolysis is indicated in blue. (For interpretation of the references to color in this figure legend, the reader is referred to the web version of this article.).

through FBA and FBP reactions. Note that *Synechocystis* contains two FBAs: CI-FBA with higher reactivity for fructose-bisphosphate and CII-FBA with higher reactivity for sedoheptulose-bisphosphate. CI-FBA has been shown to be non-essential during photoautotrophic growth of *Synechocystis* (Nakahara et al., 2003). It has been suggested that over 90% of the FBA in *Synechocystis* under photoautotrophic growth conditions is CII-FBA (Liang and Lindblad, 2016), consistent with the fact that CII-FBA has a 3-fold higher transcriptomic abundance (Saha et al., 2016) and a 39-fold higher proteomic abundance (Takabayashi et al., 2013) compared to CI-FBA. These findings support an inactive CI-FBA which results in the absence of flux through the fructose bisphosphate aldolase and fructose-bisphosphatase reactions. As a consequence of this, hexose phosphates for glycogen synthesis can only be synthesized via the TAL reaction. This increased flux through TAL is consistent with the experimentally observed higher expression levels of the *tal* gene during photoautotrophic growth phase in *Synechocystis* (Kucho et al., 2005). In order to assess the impact of the higher flux through the TAL reaction on the quality of fit, flux elucidation was performed using *i*mSyn617 upon constraining the flux through TAL to zero. Removal of the TAL reaction redirects carbon flux through the FBA/FBP route and the oxidative pentose phosphate pathway. Since the TAL reaction participates in a cycle involving a conserved E4P moiety, flux through this cycle delays the ^{13}C incorporation into sugar phosphate intermediates in the CBB cycle. This delay is not possible via the FBA/FBP route and therefore increases the SSRES to 541 due to poorly recapitulated labeling dynamics of R5P229 and RuBP309 fragments (Supplementary Fig. S4). The best fit obtained using *i*mSyn617 leading to a statistically significant reduction in SSRES requires flux through the TAL reaction ($F = 16.32$, $p = 6.1\times10^{-5}$). In comparison, the core model uses the traditional CBB pathway for pentose phosphate regeneration, resulting in a flux of 58 mmol/dmol BCU through FBA and FBP reactions while the directionality of TAL remains unresolved.

While both models assume the same biomass macromolecular compositions, differences in precursor drains result in significant flux range shifts downstream to carbon fixation in the core and *i*mSyn617 models. In particular, lipids are traced indirectly only through free fatty

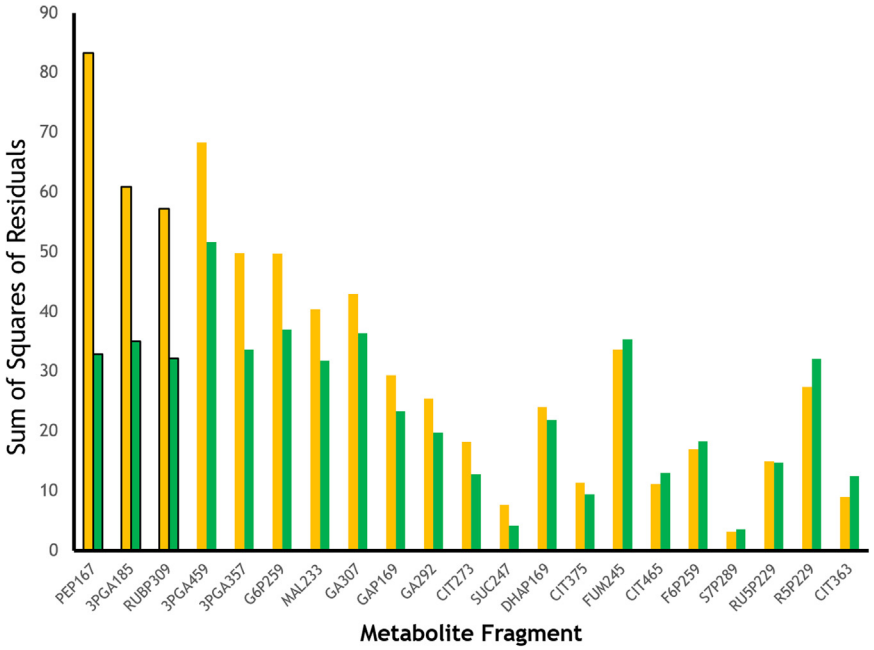

Fig. 3. Recapitulation of experimentally measured labeling distribution and dynamics expressed in terms of variance-weighted sum of squares of residuals (SSRES) using the core model (orange bars) and the GSMM model (green bars) of *Synechocystis*. Fragments with an SSRES difference exceeding 25 are indicated using a black box. (For interpretation of the references to color in this figure legend, the reader is referred to the web version of this article.).

acids in the core model as opposed to a complete coverage of glycolipids, di- and triacylglycerols (DAGs and TAGs), phospholipids, and sulfoquinovosyl DAGs in *i*mSyn617. This results in a reduced acetyl-CoA demand and an increased DHAP demand for biomass production in *i*mSyn617. As a consequence, a 50%, 89%, and 67% reduction in flux is predicted through lower glycolysis, PK, and PDH reactions, respectively. In addition to this, the core model uses the glyoxylate shunt as a secondary source of glyoxylate, thereby enabling completion of the TCA cycle without including the AKGDH reaction. In contrast, the glyoxylate shunt is excluded from *i*Syn731 as this pathway is shown to be absent in *Synechocystis* (Thiel et al., 2017) resulting in glyoxylate production only in the photorespiratory pathway. Furthermore, *i*Syn731 accounts for multiple avenues for the completion of the TCA cycle via AKGDH and its alternate routes and captures glycine and serine metabolism, thereby elucidating parts of the metabolic network not captured by the core model.

3.3. New insight on carbon paths gained using imSyn617

The overall carbon balance reveals that 86% of the assimilated bicarbonate is channeled towards biomass production, 12% is ultimately off-gassed as CO_2 and the remaining 2% is distributed between organic acids and glycogen storage. 602 reactions are resolved with a flux range narrower than 10 mmol/dmol BCU. 407 reactions are identified to be growth-coupled. These flux ranges were compared to flux ranges generated using FVA upon constraining the bounds of substrate uptake and product yields with MFA-derived lower and upper bounds. The superior flux resolution afforded by INST-MFA compared to simply FVA is attributed to the unambiguous elucidation of fluxes across all branch-points such as CBB cycle/photorespiration, glycolysis/PP pathway, anaplerotic reactions, and the TCA cycle. In addition to this, futile cycles involving central metabolic reactions such as PK, GAK, and PFK are well resolved with zero flux using INST-MFA compared to FVA based on their contribution to carbon skeleton rearrangement and impact on metabolite labeling dynamics. 61 reactions outside the purview of the EMU model are poorly resolved by both INST-MFA and FVA. These include reactions from energy metabolism such as cyclic and non-cyclic photophosphorylation, Mehler reaction, and oxidative phosphorylation, and reactions facilitating reversible transfer of reducing equivalents between various carriers such as ferredoxin, NAD+ and NADP+ such as Glutamate dehydrogenase, Glutamine synthase/Glutamate: Oxoglutarate aminotransferase system, and isozymes of glyceraldehyde-3-phosphate dehydrogenase. The expanded pathway coverage in *i*Syn731 provides insights into carbon flows through various pathways not modeled in the core model such as aspartate, glutamate, glycine, and serine metabolism and reveals the existence of pathway topologies supporting carbon conversion to biomass with near 100% efficiency.

Glycine and serine metabolism exhibits a bifurcated topology involving reactions from the photorespiratory pathway, the phosphoserine pathway, and SHMT (Fig. 5a). Flux through the carboxylation and oxygenation reactions of RuBisCO is partitioned in a 90:10 ratio with 9.7 mmol/dmol BCU of flux entering the photorespiratory pathway (Fig. 4). Oxygenation of RuBP produces one molecule 3PG and one molecule of 2PGLYC, which is oxidized to glyoxylate in the photorespiratory pathway (Fig. 5a). Since no oxidation of glyoxylate to formate or CO_2 occurs, all of the 2PGLYC synthesized via oxidation of RuBP is converted to glycine. Absence of flux through glyoxylate oxidation is supported by experimentally observed insignificant ^{13}C incorporation into oxalate (Young et al., 2011). 3PG is converted to serine via the phosphoserine (PHSER) pathway similar to *E. coli*. Glycine is also produced from serine via the SHMT reaction. Since *Synechocystis* does not accumulate or secrete glycine, and no glycine degradation occurs via GLYDH, it is exclusively utilized for biomass production, as a result of which, the glycine producing branch of the photorespiratory pathway is identified to be growth-coupled. Moreover, the SHMT reaction is identified to be the sole source of the one-carbon pool carried by tetrahydrofolate. A trace flux is observed through glycerate indicating that the second half of the photorespiratory pathway is inactive (Supplementary File 1) causing the phosphoserine pathway to be growth-coupled. This flux distribution results in a unique bifurcated topology achieving complete carbon conversion of RuBP to glycine and serine with no losses in the form of CO_2. Furthermore, cysteine is also synthesized from serine and completely routed to biomass as there is no flux through the cysteine-degrading mercaptopyruvate pathway (Supplementary File 1). The overall topology of this pathway allows glycine and serine biosynthesis from bicarbonate with a 100% carbon conversion efficiency while reinforcing the essentiality of the glycolate pathway in *Synechocystis* (Eisenhut et al., 2008). This observation is in contrast to the linear pathway proposed in earlier GSM models of *Synechocystis* (Knoop et al., 2010) and affords a higher ^{13}C enrichment of serine than glycine, consistent with experimental observations (Huege

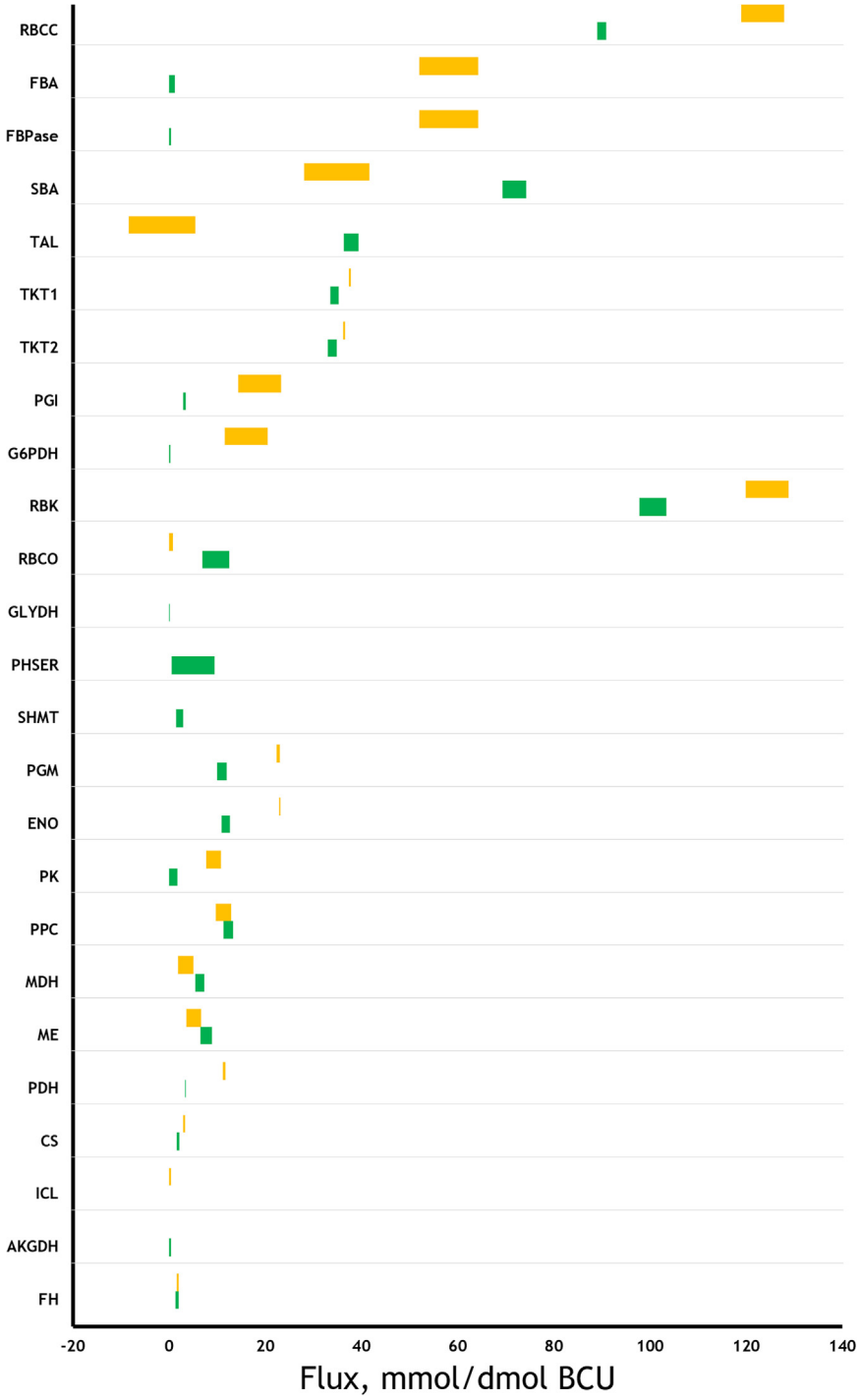

Fig. 4. Flux ranges (expressed in mmol/dmol bicarbonate uptake (BCU)) of central metabolic reactions in *Synechocystis* during photoautotrophic growth predicted using a core model (orange bars) and a GSMM model (green bars). The bars represent the range of flux from its lower bound to its upper bound. The reaction names on the y-axis are consistent with the nomenclature used in Fig. 1. Excluded reactions in each model are assumed to carry no flux. (For interpretation of the references to color in this figure legend, the reader is referred to the web version of this article.).

et al., 2007; Young et al., 2011).

The genome-scale mapping model *i*mSyn617 achieves an unambiguous resolution of fluxes around the pyruvate node (Fig. 4). Pyruvate synthesis occurs indirectly from PEP via the anaplerotic PPC and ME reactions due to the inactivity of PK, methylglyoxal, and serine degradation pathways. In addition to this, no flux is seen through the PPS reaction indicating unidirectional flux from glycolysis to the TCA cycle, thereby localizing any CO_2 incorporated via PPC to the TCA cycle only. Acetyl-CoA is produced via the PDH reaction for lipid synthesis and TCA metabolism. Absence of flux through all alternate routes connecting AKG and succinate in conjunction with the lack of a glyoxylate shunt (Thiel et al., 2017; Varman et al., 2013) renders the TCA cycle incomplete with a bifurcated topology incapable of completely oxidizing acetyl-CoA (Fig. 4b). As a consequence, all reactions of the TCA cycle are identified to be growth coupled as *Synechocystis* does not produce any organic acids as byproducts of photoautotrophic metabolism (Young et al., 2011). Fumarate is not synthesized directly via the TCA cycle, but is instead generated as a byproduct of arginine and

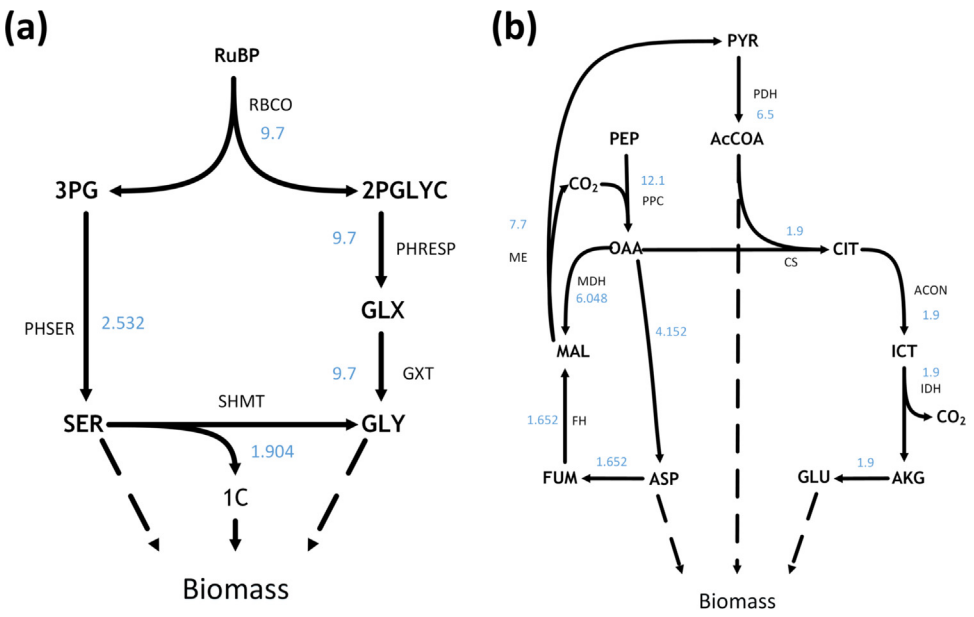

Fig. 5. Bifurcated topology of the photorespiratory pathway (a) and the TCA cycle (b). Flux (in mmol/dmol BCU) through each reaction is specified adjacent to the reaction abbreviation. Arrows indicate direction of flux. Reaction abbreviations are consistent with Fig. 1. The dashed arrows represent metabolite drains for biomass production.

purine biosynthetic pathways. This fumarate serves as a precursor for succinate required for growth, while the excess fumarate is converted to malate via fumarate hydratase.

4. Discussion

In this study, genome-scale INST-MFA is applied to elucidate photoautotrophic metabolism in *Synechocystis*. Reactions capable of carrying flux in *i*Syn731 (Saha et al., 2012) are identified via FVA using extracellular flux measurement data (Young et al., 2011). The corresponding GSMM model *i*mSyn617 includes all carbon-balanced reactions Atom mapping for reactions shared with *E. coli* is derived from *i*mEco726 (Gopalakrishnan and Maranas, 2015a) and the remaining reactions are mapped using the CLCA algorithm or based on reaction mechanism when available. A customized algorithm is developed with improved scalability and memory efficiency leading to a 48% reduction per iteration in the computational time required to simulate of metabolite labeling dynamics in larger networks. INST-MFA is performed to identify a suitable flux distribution accurately recapitulating the labeling distribution and dynamics of 15 central metabolites obtained during photoautotrophic growth of *Synechocystis* with 50% ^{13}C-labeled bicarbonate as the tracer (Young et al., 2011). In response to degeneracy in the metabolic network and experimental errors, 95% confidence intervals were also determined using the established procedure (Antoniewicz et al., 2006; Gopalakrishnan and Maranas, 2015a) to identify flux ranges for all reactions.

Upon evaluating the significance of the improved recapitulation afforded by *i*mSyn617 using the *F*-test, the F-statistic is 1.335 ($p = 0.012$). In comparison, the corresponding F-statistic for scale-up in *E. coli* was 0.152 ($p = 0.999$) indicating that the core model accounts for the carbon paths necessary to recapitulate the labeling data used in that study (Gopalakrishnan and Maranas, 2015a). The increased uncertainty of flux estimation was attributed to the inclusion of alternate paths with identical atom mapping information. In contrast, the statistical significance associated with model scale-up in this study implies that unique and often surprising insights into the carbon flows under phototrophic growth are obtained by the re-analysis of an existing dataset using a detailed description of the entirety of metabolism in *Synechocystis*. Interestingly, both the core model and *i*mSyn617 report two qualitatively different flux distributions that are within the acceptable χ^2 statistical threshold. While a statistically significant reduction in SSRES is seen upon permitting flux through the oxidative pentose phosphate pathway in the core model (Supplementary Fig. S3), *i*mSyn617 supports a statistically significant improvement in solution quality upon permitting flux through the TAL reaction which in turn reduces the flux through the oxidative pentose phosphate pathway to zero (Supplementary Fig. S4). As a result of this, unambiguous resolution of the flux through the oxidative pentose phosphate pathway requires 13C-labeling measurements for 6PG during flux elucidation using INST-MFA. Pool size measurements for 6PG under photoautotrophic growth conditions have already been quantified using metabolomics (Yoshikawa et al., 2013). Resolution of the flux through the oxidative pentose phosphate pathway will provide insights into whether this pathway is regulated at the transcriptomic level (Kucho et al., 2005) or at the post-translational level (Knowles and Plaxton, 2003) and provide a clearer explanation for the reported non-essentiality of the *zwf* and *gnd* genes (Scanlan et al., 1995; Wan et al., 2017) under photoautotrophic growth conditions. Flux elucidation under photoautotrophic growth conditions using *i*mSyn617 reveals that *Synechocystis* deploys a carbon efficient metabolism enabling maximal conversion of fixed carbons to biomass precursors with minimal production of organic acids and glycogen. This is in contrast to heterotrophic bacteria such as *E. coli* where 35% of the taken-up glucose is secreted as acetate (Sandberg et al., 2016) resulting in a 30% biomass yield loss from the theoretical maximum biomass yield (Feist et al., 2007). The flux ranges estimated in this study provide a comprehensive set of essential and dispensable metabolic reactions in *Synechocystis* under photoautotrophic growth conditions to serve as a guideline for editing photosynthetic prokaryotic genomes. The estimated flux ranges reveal that only 88% of the fixed bicarbonate is ultimately routed towards biomass production. 12% of the fixed carbons are oxidized to CO_2 via anabolic reactions essential for biomass production. Flux elucidation using INST-MFA reveals that these carbons are not recycled by RuBisCO and are subsequently off-gassed. This inability to recycle these carbons via the CBB cycle results in a 12% reduction in biomass yield compared to predictions using flux balance analysis (Supplementary File 1). In order to determine whether this absence of CO_2 recycling is the only cause of loss in biomass yield, the maximum biomass yield was calculated using flux balance analysis upon constraining the flux through RuBisCO to the range estimated using INST-MFA. The maximum biomass yield was calculated to be 2.48 gDW/dmol BCU, which is 2% greater than the biomass yield estimated using INST-MFA (Supplementary File 1). Based on this, we confirm that *Synechocystis* possesses an efficient metabolism enabling a near-perfect routing of

fixed carbons towards biomass precursors. However, it is unclear from this analysis whether the inability to recycle oxidized carbons is caused by a rate-limiting enzyme in the CBB cycle or a paucity of available NADPH and ATP as the fluxes through the photosynthetic light reactions and oxidative phosphorylation are poorly resolved by INST-MFA. Resolution of these reactions requires knowledge of the spectral composition of the light source and photon flux partitioning between photosystems I and II to distinguish ATP production via non-cyclic and cyclic photophosphorylation. When combined with the measurement of net oxygen evolution rate, these measurements will allow accurate elucidation of fluxes through the photosynthetic light reactions and oxidative phosphorylation. This will enable resolution of NADPH production and provide insights into the biological impact of a mandatory flux through Malic Enzyme, consistent with experimentally verified essentiality of this gene (Bricker et al., 2004). Unlike in *E. coli* (Gopalakrishnan and Maranas, 2015a), here alternate routes to lower glycolysis and TCA cycle are extremely well resolved based on differences in metabolite labeling dynamics, thereby demonstrating the superior capability of INST-MFA in resolving pathways with similar atom transitions and establishing the dispensability of the lower TCA cycle under photoautotrophic growth conditions.

The introduced algorithmic procedure (Supplementary material) for performing flux elucidation at a genome-scale offers a 48% reduction in computation time which will grow with larger models. As this scheme employs an exponential integrator, a moderate level of stiffness can still be handled when pool sizes exceed 10^{-4} mmol/gdw. Stiffness in INST-MFA models arises from a degeneracy in pathway labeling dynamics due to the inclusion of more pool size parameters than necessary to recapitulate experimentally observed labeling distributions. As a consequence of this, the confidence interval estimation procedure will fail to compute an upper bound for many metabolite turnover rates (defined as the ratio of flux through a metabolite to its pool size). Since fluxes are scaled to bicarbonate uptake and bounded by stoichiometric mass balance constraints, the uncertainties in the estimation of metabolite turnover rates will be reflected in uncertainties in pool size resolution but does not affect flux confidence interval calculation as long as the solution lies outside the stiff regions. Due to this, pool size ranges are not computed in this study. This would require the development of a higher order implicit method for ODE integration so as to ensure accuracy and stability of the procedure. It has been previously reported that channeling plays a key role in explaining the observed metabolite labeling dynamics (Huege et al., 2007; Young et al., 2011). The presence of substrate channeling was hypothesized based on the existence of segregated metabolite pools inferred from dilution parameters (Young et al., 2011). Consistent with earlier findings, up to 10% of the 3PG and F6P pools are found to be metabolically inactive with no segregation of the PEP pool, alluding to the presence of a channeling mechanism from 3PG to PEP. Quantification of pool sizes will provide detailed insights into substrate channeling mechanisms arising from CBB cycle enzyme co-localization similar to that seen in plant chloroplasts (Anderson and Carol, 2004; Anderson et al., 2005; Suss et al., 1993). In conjunction with the bi-functionality of the SBPase enzyme (Yan and Xu, 2008), this would explain the preference for TAL-SBPase-SBA route for the regeneration of pentose sugar phosphates as opposed to the conventional TPI-FBA-FBPase pathway despite the lack of an energetic advantage. Nevertheless, the flux estimation algorithm always converged outside the stiff regions in the solution space, indicating that the obtained flux ranges are not confounded by stiffness of the system of ODEs describing metabolite labeling dynamics in GSM models. *i*mSyn617 coupled with customized integrators enables the elucidation of fluxes with a global coverage and high statistical confidence by re-analyzing already available labeling datasets. This newly reached scope and fidelity in flux elucidation promises to enhance both kinetic model parametrization (Khodayari and Maranas, 2016) and facilitate the use of strain design algorithms such as OptForce (Ranganathan et al., 2010), and k-OptForce (Chowdhury et al., 2014).

Acknowledgement

This work was supported by the U.S. Department of Energy (DOE) under Grants DE-SC10822882 and DE-FG02-05ER25684 and NSF/MCB-1546840.

Appendix A. Supplementary material

Supplementary data associated with this article can be found in the online version at doi:10.1016/j.ymben.2018.03.008.

References

Abernathy, M.H., Yu, J., Ma, F., Liberton, M., Ungerer, J., Hollinshead, W.D., Gopalakrishnan, S., He, L., Maranas, C.D., Pakrasi, H.B., et al., 2017. Deciphering cyanobacterial phenotypes for fast photoautotrophic growth via isotopically non-stationary metabolic flux analysis. Biotechnol. Biofuels 10, 273.

Alagesan, S., Gaudana, S.B., Sinha, A., Wangikar, P.P., 2013. Metabolic flux analysis of Cyanothece sp. ATCC 51142 under mixotrophic conditions. Photosynth. Res. 118, 191–198.

Anderson, L.E., Carol, A.A., 2004. Enzyme co-localization with rubisco in pea leaf chloroplasts. Photosynth. Res. 82, 49–58.

Anderson, L.E., Gatla, N., Carol, A.A., 2005. Enzyme co-localization in pea leaf chloroplasts: glyceraldehyde-3-p dehydrogenase, triose-P isomerase, aldolase and sedoheptulose bisphosphatase. Photosynth. Res. 83, 317–328.

Antoniewicz, M.R., Kelleher, J.K., Stephanopoulos, G., 2006. Determination of confidence intervals of metabolic fluxes estimated from stable isotope measurements. Metab. Eng. 8, 324–337.

Antoniewicz, M.R., Kelleher, J.K., Stephanopoulos, G., 2007. Elementary metabolite units (EMU): a novel framework for modeling isotopic distributions. Metab. Eng. 9, 68–86.

Atsumi, S., Higashide, W., Liao, J.C., 2009. Direct photosynthetic recycling of carbon dioxide to isobutyraldehyde. Nat. Biotechnol. 27, 1177–1180.

Bricker, T.M., Zhang, S., Laborde, S.M., Mayer 3rd, P.R., Frankel, L.K., Moroney, J.V., 2004. The malic enzyme is required for optimal photoautotrophic growth of Synechocystis sp. strain PCC 6803 under continuous light but not under a diurnal light regimen. J. Bacteriol. 186, 8144–8148.

Chen, W.L., Chen, D.Z., Taylor, K.T., 2013. Automatic reaction mapping and reaction center detection. Wiley Interdiscip. Rev.: Comput. Mol. Sci. 3, 560–593.

Chen, X., Schreiber, K., Appel, J., Makowka, A., Fähnrich, B., Roettger, M., Hajirezaei, M.R., Sönnichsen, F.D., Schönheit, P., Martin, W.F., et al., 2016. The Entner–Doudoroff pathway is an overlooked glycolytic route in cyanobacteria and plants. Proc. Natl. Acad. Sci. USA 113, 5441–5446.

Chowdhury, A., Zomorrodi, A.R., Maranas, C.D., 2014. k-OptForce: integrating kinetics with flux balance analysis for strain design. PLoS Comput. Biol. 10, e1003487.

Eisenhut, M., Ruth, W., Haimovich, M., Bauwe, H., Kaplan, A., Hagemann, M., 2008. The photorespiratory glycolate metabolism is essential for cyanobacteria and might have been conveyed endosymbiontically to plants. Proc. Natl. Acad. Sci. USA 105, 17199–17204.

Feist, A.M., Henry, C.S., Reed, J.L., Krummenacker, M., Joyce, A.R., Karp, P.D., Broadbelt, L.J., Hatzimanikatis, V., Palsson, B.O., 2007. A genome-scale metabolic reconstruction for Escherichia coli K-12 MG1655 that accounts for 1260 ORFs and thermodynamic information. Mol. Syst. Biol. 3, 121.

Feng, X., Bandyopadhyay, A., Berla, B., Page, L., Wu, B., Pakrasi, H.B., Tang, Y.J., 2010. Mixotrophic and photoheterotrophic metabolism in Cyanothece sp. ATCC 51142 under continuous light. Microbiology 156, 2566–2574.

Franklin, G.F., Powell, D.J., Workman, M.L., 1997. Digital Control of Dynamic Systems, 3rd ed. Addison-Wesley Longman Publishing Co., Inc., Boston, MA, USA.

Gill, P.E., Murray, W., Wright, M.H., 1984. Practical Optimization. Academic Press, London.

Giuliano, G., 2014. Plant carotenoids: genomics meets multi-gene engineering. Curr. Opin. Plant Biol. 19, 111–117.

Gopalakrishnan, S., Maranas, C.D., 2015a. 13C metabolic flux analysis at a genome-scale. Metab. Eng. 32, 12–22.

Gopalakrishnan, S., Maranas, C.D., 2015b. Achieving metabolic flux analysis for S. cerevisiae at a genome-scale: challenges, requirements, and considerations. Metabolites 5, 521–535.

Hasunuma, T., Kikuyama, F., Matsuda, M., Aikawa, S., Izumi, Y., Kondo, A., 2013. Dynamic metabolic profiling of cyanobacterial glycogen biosynthesis under conditions of nitrate depletion. J. Exp. Bot. 64, 2943–2954.

Huege, J., Goetze, J., Schwarz, D., Bauwe, H., Hagemann, M., Kopka, J., 2011. Modulation of the major paths of carbon in photorespiratory mutants of synechocystis. PLoS One 6, e16278.

Huege, J., Sulpice, R., Gibon, Y., Lisec, J., Koehl, K., Kopka, J., 2007. GC-EI-TOF-MS analysis of in vivo carbon-partitioning into soluble metabolite pools of higher plants by monitoring isotope dilution after 13CO2 labelling. Phytochemistry 68, 2258–2272.

Jochum, C., Gasteiger, J., Ugi, I., 1980. The principle of minimum chemical distance (PMCD). Angew. Chem. Int. Ed. Engl. 19, 495–505.

Khodayari, A., Maranas, C.D., 2016. A genome-scale Escherichia coli kinetic metabolic model k-ecoli457 satisfying flux data for multiple mutant strains. Nat. Commun. 7, 13806.

Klemke, F., Baier, A., Knoop, H., Kern, R., Jablonsky, J., Beyer, G., Volkmer, T., Steuer, R.,

Lockau, W., Hagemann, M., 2015. Identification of the light-independent phosphoserine pathway as an additional source of serine in the cyanobacterium Synechocystis sp. PCC 6803. Microbiology 161, 1050–1060.
Knoop, H., Zilliges, Y., Lockau, W., Steuer, R., 2010. The metabolic network of Synechocystis sp. PCC 6803: systemic properties of autotrophic growth. Plant Physiol. 154, 410–422.
Knowles, V.L., Plaxton, W.C., 2003. From genome to enzyme: analysis of key glycolytic and oxidative pentose-phosphate pathway enzymes in the cyanobacterium Synechocystis sp. PCC 6803. Plant Cell Physiol. 44, 758–763.
Kucho, K., Okamoto, K., Tsuchiya, Y., Nomura, S., Nango, M., Kanehisa, M., Ishiura, M., 2005. Global analysis of circadian expression in the cyanobacterium Synechocystis sp. strain PCC 6803. J. Bacteriol. 187, 2190–2199.
Kumar, A., Maranas, C.D., 2014. CLCA: maximum common molecular substructure queries within the MetRxn database. J. Chem. Inf. Model 54, 3417–3438.
Kumar, A., Suthers, P.F., Maranas, C.D., 2012. MetRxn: a knowledgebase of metabolites and reactions spanning metabolic models and databases. BMC Bioinforma. 13, 6.
Latendresse, M., Malerich, J.P., Travers, M., Karp, P.D., 2012. Accurate atom-mapping computation for biochemical reactions. J. Chem. Inf. Model 52, 2970–2982.
Leighty, R.W., Antoniewicz, M.R., 2012. Parallel labeling experiments with [U-13C]glucose validate E. coli metabolic network model for 13C metabolic flux analysis. Metab. Eng. 14, 533–541.
Liang, F., Lindblad, P., 2016. Effects of overexpressing photosynthetic carbon flux control enzymes in the cyanobacterium Synechocystis PCC 6803. Metab. Eng. 38, 56–64.
Madsen, K., Nielsen, H.B., Tingleff, O., 2004. Methods for Non-Linear Least Squares Problems, 2nd ed. Technical University of Denmark, Kongens Lyngby.
Mahadevan, R., Schilling, C.H., 2003. The effects of alternate optimal solutions in constraint-based genome-scale metabolic models. Metab. Eng. 5, 264–276.
Maurino, V.G., Weber, A.P., 2013. Engineering photosynthesis in plants and synthetic microorganisms. J. Exp. Bot. 64, 743–751.
McCloskey, D., Young, J.D., Xu, S., Palsson, B.O., Feist, A.M., 2016. Modeling method for increased precision and scope of directly measurable fluxes at a genome-scale. Anal. Chem. 88, 3844–3852.
Metallo, C.M., Walther, J.L., Stephanopoulos, G., 2009. Evaluation of 13C isotopic tracers for metabolic flux analysis in mammalian cells. J. Biotechnol. 144, 167–174.
Morgan, H.L., 1965. The generation of a unique machine description for chemical structures-A technique developed at chemical abstracts service. J. Chem. Doc. 5, 107–113.
Nakahara, K., Yamamoto, H., Miyake, C., Yokota, A., 2003. Purification and characterization of class-I and class-II fructose-1,6-bisphosphate aldolases from the cyanobacterium Synechocystis sp. PCC 6803. Plant Cell Physiol. 44, 326–333.
Nogales, J., Gudmundsson, S., Knight, E.M., Palsson, B.O., Thiele, I., 2012. Detailing the optimality of photosynthesis in cyanobacteria through systems biology analysis. Proc. Natl. Acad. Sci. USA 109, 2678–2683.
Noh, K., Wahl, A., Wiechert, W., 2006. Computational tools for isotopically instationary 13C labeling experiments under metabolic steady state conditions. Metab. Eng. 8, 554–577.
Noh, K., Wiechert, W., 2011. The benefits of being transient: isotope-based metabolic flux analysis at the short time scale. Appl. Microbiol. Biotechnol. 91, 1247–1265.
Ranganathan, S., Suthers, P.F., Maranas, C.D., 2010. OptForce: an optimization procedure for identifying all genetic manipulations leading to targeted overproductions. PLoS Comput. Biol. 6, e1000744.
Saha, R., Liu, D., Hoynes-O'Connor, A., Liberton, M., Yu, J., Bhattacharyya-Pakrasi, M., Balassy, A., Zhang, F., Moon, T.S., Maranas, C.D., et al., 2016. Diurnal regulation of cellular processes in the Cyanobacterium Synechocystis sp. strain PCC 6803: insights from transcriptomic, fluxomic, and physiological analyses. MBio 7.
Saha, R., Verseput, A.T., Berla, B.M., Mueller, T.J., Pakrasi, H.B., Maranas, C.D., 2012. Reconstruction and comparison of the metabolic potential of cyanobacteria Cyanothece sp. ATCC 51142 and Synechocystis sp. PCC 6803. PLoS One 7, e48285.
Sandberg, T.E., Long, C.P., Gonzalez, J.E., Feist, A.M., Antoniewicz, M.R., Palsson, B.O., 2016. Evolution of E. coli on [U-13C]glucose reveals a negligible isotopic influence on metabolism and physiology. PLoS One 11, e0151130.
Sauer, U., 2006. Metabolic networks in motion: 13C-based flux analysis. Mol. Syst. Biol. 2, 62.
Scanlan, D.J., Sundaram, S., Newman, J., Mann, N.H., Carr, N.G., 1995. Characterization of a zwf mutant of Synechococcus sp. strain PCC 7942. J. Bacteriol. 177, 2550–2553.
Schellenberger, J., Lewis, N.E., Palsson, B.O., 2011. Elimination of thermodynamically infeasible loops in steady-state metabolic models. Biophys. J. 100, 544–553.
Shastri, A.A., Morgan, J.A., 2007. A transient isotopic labeling methodology for 13C metabolic flux analysis of photoautotrophic microorganisms. Phytochemistry 68, 2302–2312.
Steinhauser, D., Fernie, A.R., Araujo, W.L., 2012. Unusual cyanobacterial TCA cycles: not broken just different. Trends Plant Sci. 17, 503–509.
Suss, K.H., Arkona, C., Manteuffel, R., Adler, K., 1993. Calvin cycle multienzyme complexes are bound to chloroplast thylakoid membranes of higher plants in situ. Proc. Natl. Acad. Sci. USA 90, 5514–5518.
Suthers, P.F., Burgard, A.P., Dasika, M.S., Nowroozi, F., Van Dien, S., Keasling, J.D., Maranas, C.D., 2007. Metabolic flux elucidation for large-scale models using 13C labeled isotopes. Metab. Eng. 9, 387–405.
Takabayashi, A., Kadoya, R., Kuwano, M., Kurihara, K., Ito, H., Tanaka, R., Tanaka, A., 2013. Protein co-migration database (PCoM -DB) for Arabidopsis thylakoids and Synechocystis cells. Springerplus 2, 148.
Tang, Y.J., Martin, H.G., Myers, S., Rodriguez, S., Baidoo, E.E., Keasling, J.D., 2009. Advances in analysis of microbial metabolic fluxes via (13)C isotopic labeling. Mass Spectrom. Rev. 28, 362–375.
Thiel, K., Vuorio, E., Aro, E.M., Kallio, P.T., 2017. The effect of enhanced acetate influx on Synechocystis sp. PCC 6803 metabolism. Microb. Cell Fact. 16, 21.
Varman, A.M., Yu, Y., You, L., Tang, Y.J., 2013. Photoautotrophic production of D-lactic acid in an engineered cyanobacterium. Microb. Cell Fact. 12, 117.
Wan, N., DeLorenzo, D.M., He, L., You, L., Immethun, C.M., Wang, G., Baidoo, E.E.K., Hollinshead, W., Keasling, J.D., Moon, T.S., et al., 2017. Cyanobacterial carbon metabolism: fluxome plasticity and oxygen dependence. Biotechnol. Bioeng. 114, 1593–1602.
Wiechert, W., Mollney, M., Isermann, N., Wurzel, M., de Graaf, A.A., 1999. Bidirectional reaction steps in metabolic networks: iii. Explicit solution and analysis of isotopomer labeling systems. Biotechnol. Bioeng. 66, 69–85.
Wiechert, W., Wurzel, M., 2001. Metabolic isotopomer labeling systems. Part I: global dynamic behavior. Math. Biosci. 169, 173–205.
Xiong, W., Morgan, J.A., Ungerer, J., Wang, B., Maness, P.-C., Yu, J., 2015. The plasticity of cyanobacterial metabolism supports direct CO_2 conversion to ethylene. Nat. Plants 1, 15053.
Yan, C., Xu, X., 2008. Bifunctional enzyme FBPase/SBPase is essential for photoautotrophic growth in cyanobacterium Synechocystis sp. PCC 6803. Prog. Nat. Sci. 18, 149–153.
Yang, C., Hua, Q., Shimizu, K., 2002a. Integration of the information from gene expression and metabolic fluxes for the analysis of the regulatory mechanisms in Synechocystis. Appl. Microbiol. Biotechnol. 58, 813–822.
Yang, C., Hua, Q., Shimizu, K., 2002b. Metabolic flux analysis in Synechocystis using isotope distribution from 13C-labeled glucose. Metab. Eng. 4, 202–216.
Yang, C., Hua, Q., Shimizu, K., 2002c. Quantitative analysis of intracellular metabolic fluxes using GC-MS and two-dimensional NMR spectroscopy. J. Biosci. Bioeng. 93, 78–87.
Yoshikawa, K., Hirasawa, T., Ogawa, K., Hidaka, Y., Nakajima, T., Furusawa, C., Shimizu, H., 2013. Integrated transcriptomic and metabolomic analysis of the central metabolism of Synechocystis sp. PCC 6803 under different trophic conditions. Biotechnol. J. 8, 571–580.
You, L., Berla, B., He, L., Pakrasi, H.B., Tang, Y.J., 2014. 13C-MFA delineates the photomixotrophic metabolism of Synechocystis sp. PCC 6803 under light- and carbon-sufficient conditions. Biotechnol. J. 9, 684–692.
Young, J.D., Shastri, A.A., Stephanopoulos, G., Morgan, J.A., 2011. Mapping photoautotrophic metabolism with isotopically nonstationary (13)C flux analysis. Metab. Eng. 13, 656–665.
Young, J.D., Walther, J.L., Antoniewicz, M.R., Yoo, H., Stephanopoulos, G., 2008. An elementary metabolite unit (EMU) based method of isotopically nonstationary flux analysis. Biotechnol. Bioeng. 99, 686–699.
Yu, Y., You, L., Liu, D., Hollinshead, W., Tang, Y.J., Zhang, F., 2013. Development of Synechocystis sp. PCC 6803 as a phototrophic cell factory. Mar. Drugs 11, 2894–2916.
Zhang, S., Bryant, D.A., 2011. The tricarboxylic acid cycle in cyanobacteria. Science 334, 1551–1553.
Zomorrodi, A.R., Maranas, C.D., 2010. Improving the iMM904 S. cerevisiae metabolic model using essentiality and synthetic lethality data. BMC Syst. Biol. 4, 178.
Zomorrodi, A.R., Suthers, P.F., Ranganathan, S., Maranas, C.D., 2012. Mathematical optimization applications in metabolic networks. Metab. Eng. 14, 672–686.